PERGAMON

International Journal of Heat and Mass Transfer 43 (2000) 1547–1562

International Journal of HEAT and MASS TRANSFER

www.elsevier.com/locate/ijhmt

Terrestrial and microgravity boiling heat transfer in a dielectrophoretic force field

T.J. Snyder, J.N. Chung*

School of Mechanical and Materials Engineering, Washington State University, Pullman, WA 99164-2920, USA

Received 1 June 1998; received in revised form 16 July 1999

Abstract

In order to maintain steady nucleate boiling in microgravity another force must be imposed on the boiling process to replace the buoyancy force. The objective of this study is to investigate the effectiveness of a static electric field for maintaining nucleate boiling in microgravity. Semi-transparent gold-film heaters are used to measure the instantaneous average heater surface temperature and to provide a bottom view of the boiling process. Three electrode geometries are designed with this heater: a diverging plate, a flat plate, and a pin electrode. Depending on the heat flux level and voltage strength, it was found that each of these electrodes is able to effectively move the boiling bubbles away from the vicinity of the heater surface in microgravity. Both flow visualization and measured heat transfer data are obtained to verify these results.

1. Introduction

The loss of buoyancy in microgravity has been found to change the nature of terrestrial nucleate boiling, which is driven primarily by the gravity on Earth. Experiments over the past 30 years have led to the general conclusion that under specific conditions other mechanisms including inertia, surface tension, and evaporation can lead to a quasi-steady boiling process in microgravity for limited periods of time [1–3]. However, the boiling process in microgravity appears to be strongly dependent on heat flux and subcooling levels. At higher heat fluxes and/or lower levels of subcooling, the heater can become blanketed by vapor and subsequent dryout of the heater surface ensues. For example, Lee et al. [3] presented measured data obtained in a GAS experiment in the Space Shuttle. They showed that a quasi-steady boiling process can be maintained for a short period with a heat flux of 3.6×10^4 W/m^2 and a relatively large subcooling (11.9°C). Under these conditions the heat transfer coefficient was stable for up to 75 s. However, for an even smaller heat flux (1.8×10^4 W/m^2) with nearly saturated conditions (0.2°C subcooling) the heat transfer coefficient was stable for 15–20 s and then dropped due to dryout of the heater surface. It is therefore anticipated that dryout will eventually take place with any boiling under microgravity since condensation at the liquid–vapor interface serves to decrease the local subcooling unless some means is provided to lift the bubbles or move the subcooled bulk liquid to the vicinity of the liquid–vapor interface. Therefore, from an engineering standpoint, a means of removing the vapor bubbles from the immediate vicinity of the heater surface must be devised.

With the masking effects of gravity reduced to a negligible extent, other forces can be used to manipulate liquids and gases during boiling. The focus of this study is to examine experimentally the feasibility

* Corresponding author. Current address: Department of Mechanical Engineering, University of Florida, Gainsville, FL 32611-6300, USA.

0017-9310/00/$ - see front matter
PII: S0017-9310(99)00237-9

and effectiveness of a static electric field for providing a sustained force in microgravity to maintain the nucleate boiling process.

2. Theory

One generally accepted expression for the electrohydrodynamic force produced by an electric field acting on a unit volume of dielectric fluid is given by Stratton [4]:

$$\mathbf{F}^{e} = \rho_f \mathbf{E} - 0.5 \mid \mathbf{E} \mid^2 \nabla\varepsilon - \nabla\left(\frac{1}{2}\rho\left(\frac{\partial\varepsilon}{\partial\rho}\right)_T \mid \mathbf{E} \mid^2\right) \quad (1)$$

where $\mathbf{F}^e$ is the total force per unit volume, ρ_f is the free charge density, $\mathbf{E}$ is the electric field strength, ε is the dielectric permittivity, and ρ is the dielectric material density. The subscript, T, represents a constant temperature condition. The first term is the force per unit volume on a medium containing free electric charge of density ρ_f. The second term is the force per unit volume exerted on a dielectric liquid due to gradients in the permittivity. Since ε is not differentiable at a liquid–vapor interface, it is appropriate for both liquid droplets and vapor bubbles to follow directly the general formula of a dielectrophoretic force acting on a dielectric sphere in a two-phase mixture. The resulting DEP force for a vapor bubble is given by Pohl [5] and Jones and Bliss [6] as follows:

$$\mathbf{F}_{DEP} = 2\pi R^3 \varepsilon_0 \varepsilon_l \left(\frac{\varepsilon_v - \varepsilon_l}{\varepsilon_v + 2\varepsilon_l}\right) \nabla(\mid \mathbf{E} \mid^2) \quad (2)$$

where R is the radius of the bubble, and ε_o, ε_l, and ε_v are the permittivities of the free space,

liquid and vapor, respectively. The direction of this force is such that the medium with relatively smaller permittivity will be driven away from regions of high electric field towards regions of lower electric field. The third term in Eq. (1) describes electrostrictive effects. The exact physical significance of this term has been the subject of some conjecture and has been likened to an electrical pressure. Since the compressibility of a fluid is often neglected, the electrostriction effect has been considered to have no practical influence on hydrodynamics for an incompressible flow [7,8].

An experiment [6] using diverging plate electrodes to position nitrogen bubbles in Freon-113 correlated well with Eq. (2) in a static force balance. It has also been shown by Cheng and Chaddock [9], Pachosa and Chung [10], and Jones and Bliss [6] that vapor bubbles tend to elongate in the field direction and that there does exist a minimum lower size limit on particles that can be effectively moved by this polarization force.

A numerical study [11] has been performed for the divergent plates in a dielectric fluid. With the moment method, the effects of finite plate length on the force experienced by a bubble were investigated. A parametric study was also carried out where it was found that the DEP force produced by relatively high electric-field gradients is generally larger than that by lower electric-field gradients. The high electric-field gradients also allow lower voltage requirements and larger electrode spacing.

3. Experimental apparatus, test matrix, and uncertainties

3.1. Drop tower

In order to bring the buoyancy force to nearly zero and characterize the bubble dynamics, two-phase flow, and boiling heat transfer with an imposed DEP force only, a drop tower was used. The drop tower at Washington State University utilized a drag shield design and provided up to 2.1 s of microgravity. The micogravity level experienced by the experiment was measured to be approx. 10^{-5}–10^{-4} $\boldsymbol{g}$. Complete details can be found in Snyder [12].

3.2. Experimental system

The tests were conducted in the Modular Microgravity Pool and Flow Boiling Experiment (MMBE). The experiment measures 0.4 m × 0.4 m × 0.9 m and is designed to operate in the WSU 2.1 Second Drop Tower. For this study the MMBE was operated in the pool-boiling mode with the test chamber as shown in Fig. 1.

The test chamber is made of 1.27 cm thick anodized aluminum plates with bulk temperature control obtained by surface mounted KAPTON heaters on the exterior. A temperature controller and several series-T thermocouples are used at various locations to control and monitor the fluid temperature. A diaphragm stainless steel bellows is used in conjunction with a thin film pressure transducer to monitor and control the system pressure. Two 30 Hz composite video cameras were used for visualization. One is for the side view and the other for the bottom view. The electric potential was generated with a Hipotronics high-voltage d.c. power pack.

3.3. Test fluid

FC-72 was used as the working fluid for this study. FC-72 comes from a family of Fluorinert liquids [13] which are clear, colorless, odorless, non-flammable and non-explosive. This fluid also has the benefit of low

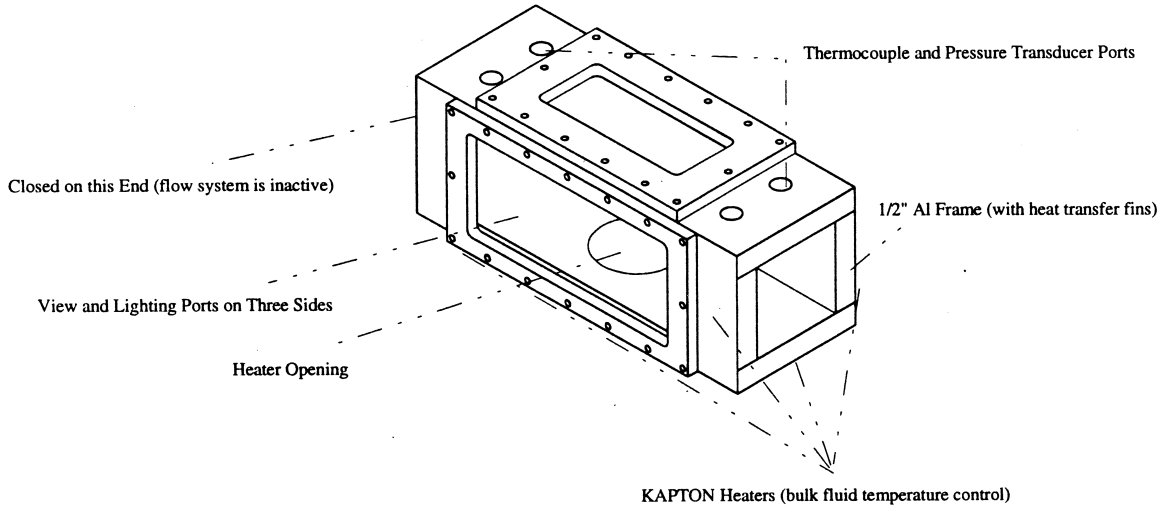

Fig. 1. Pool boiling test chamber.

toxicity and is also a highly insulating dielectric. The permittivities are approximately equal to 1.76 and 1.01 for the liquid and vapor phases, respectively. The other thennophysical properties were taken from a temperature dependent thermophysical properties chart in 3 M Product Manual [13].

A degassing procedure was followed according to the guidelines in 3 M Product Manual [13]. The procedure consisted of boiling the fluid vigorously for about twenty minutes while venting to a reflux condenser. The system was then completely sealed from the atmosphere and could be used for extended periods of time without any noticeable effect from dissolved gases, however, degassing was performed prior to each test run.

3.4. Gold-film heater

For the study of nucleate boiling of FC-72 in a microgravity environment, observation of the formation, growth, and departure of vapor bubbles from beneath the heating surface as well as from the side was desired. Along with the visualization, an instantaneous spatial average heater surface temperature was also measured that did not substantially interfere with the boiling phenomena or uncontrollably distort the electric-field distribution. This eliminated all intrusive temperature measurement techniques. The semi-transparent gold-film heater, which is approx. 400 Å in film thickness is shown in Fig. 2.

The surface-boiling gold-film heater was calibrated following Oker and Merte [14]. They found that the resistance of the gold-film holds a linear relationship with the spatially averaged surface temperature. Therefore, a calibration can be performed prior to using the heaters in which the resistance of the gold-film heater is plotted as a function of the average surface temperature. Oker and Merte [14] also noted that the y-intercept of the calibration curve for these heaters tends to shift in time. Therefore a single-point calibration was conducted prior to each experiment to determine the intercept.

3.5. Electrode geometries

The terrestrial-gravity buoyancy force is dependent on the relative density difference between the liquid and vapor phases and the orientation with respect to the heater surface. In contrast, the DEP force is dependent on the relative permittivity difference between the fluid and vapor phases and the way in which the heater surface (which served as one electrode) couples with

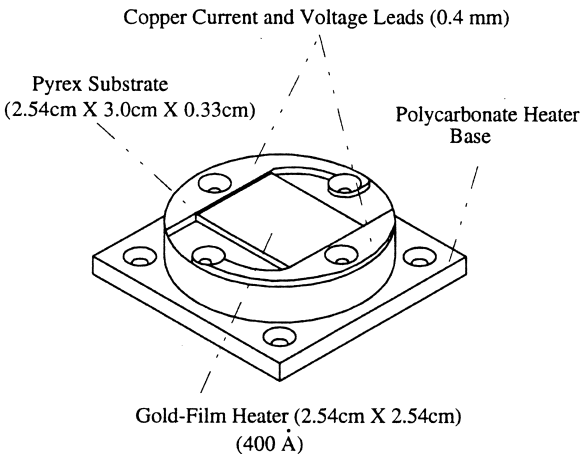

Fig. 2. Schematic of gold-film heater.

the electrode geometry. There are essentially an infinite number of possible electrode and heater geometries. As a result, there are a limitless number of possible electric-field distributions and therefore, DEP force distributions. Since the heater surface geometry was fixed (flat gold-film heater design), it became a matter of choosing appropriate electrode geometries to use in this study. Three electrode geometries were chosen which would provide a good pumping action, adequate side and bottom views of the boiling, and also a good contrast (in terms of the bubble dynamics). The three electrode geometries chosen were the diverging plate, the flat plate, and the pin electrode. A schematic of each of the heaters with the electrode mounting support structure is shown in Fig. 3.

The diverging-plate electrode was manufactured from Plexiglass and measured 2.54 cm × 2.54 cm. The plexiglass was cut at an angle at the bottom and, when mounted directly above the heater surface, formed a 13° angle with the heater surface which was of identical dimensions. The flat-plate electrode was also manufactured from plexiglass and measured 2.54 cm × 1.27 cm. The flat-plate electrode was mounted directly above the heater surface centered along both sides and was parallel with the heater surface. A thin gold-film approx. 500 Å thick was sputtered to the bottom of each of these electrodes and served as the conducting surface. This semi-transparent film was designed to provide visibility for the flow visualization of the bottom view. The gold-film also served as a fuse in the event of arcing. A countersunk hole was machined into each of the electrode surfaces. After sputtering, a brass 4-40 bolt which had been ground smooth at the top was mounted into the countersunk hole. The high voltage was provided through the contact between this bolt and the gold-film. A 10-32 threaded hole was machined into the top of each of these electrodes and served to mount the electrode to the plexiglass support structure on the heater.

The pin electrode was manufactured from a cylindrical, 5 cm long brass rod that was 3.75 mm in diameter. The top of the rod was threaded and served as a mount to the support structure and also acted as the connection for the high voltage supply. The tip of the pin electrode was rounded to 2.54 mm diameter. All the electrodes were mounted such that the distance from the heater surface to the nearest electrode position was equal to 4 mm. A factor of safety was defined in Snyder [11] and represents the degree to which the electrodes are approaching breakdown. By keeping all the minimum spacing from the electrodes to the heater surface a constant equal to 4 mm the factor of safety is satisfied for the experiments.

3.6. Test matrix

For this study a nominal subcooling of 5°C was utilized and for simplicity it will be referred to as $\Delta T_{sub} = 5°C$. The actual subcoolings for each test is given in Appendix C of Snyder [11]. Three electrode geometries were used, as discussed. For the surface-boiling study, i.e. 2.54 cm × 2.54 cm gold-film heaters, nominal heat fluxes of 3.9, 5.9 and 8.2 W/cm^2 were used with high-voltage strengths of 10, 16, and 23 kV. Again the actual heat fluxes for each test are given in Appendix C of Snyder [11]. Both microgravity and terrestrial gravity results were obtained. Table 1 provides the experimental test matrix used in these studies. For each individual run the subcooling and heat flux varied slightly. The entire test matrix is included in Appendix C of Snyder [11]. The heat flux never differed from the

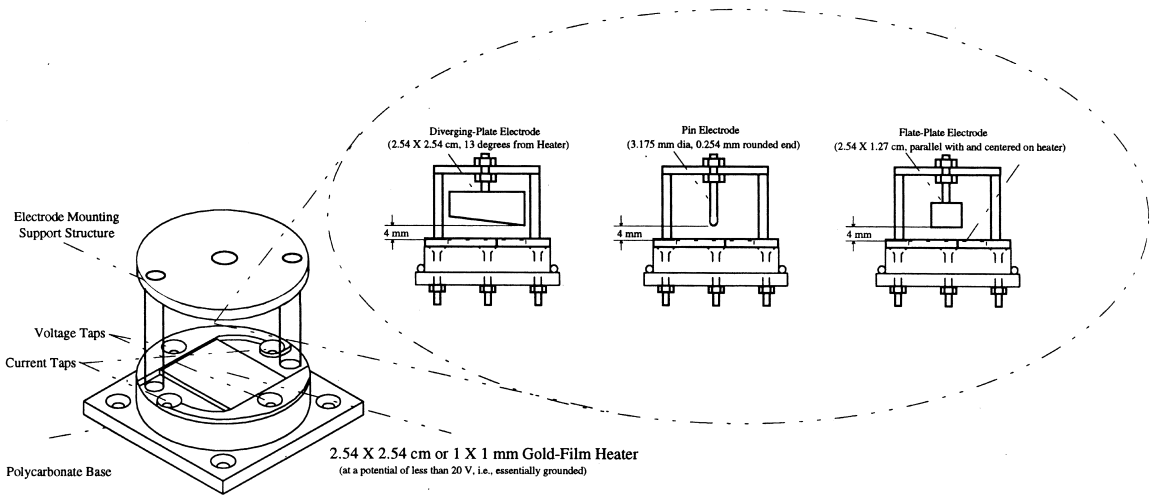

Fig. 3. Heater/electrode configurations.

Table 1
Test matrix

	High voltage (kV)	Heat flux (W/cm^2)
No electrode	0	3.9, 5.9, 8.2
Diverging plate	10	3.9, 5.9
	16	3.9, 5.9, 8.2
Flat plate	10	3.9, 5.9
	16	3.9, 5.9, 8.2
Pin electrode	10	3.9, 5.9
	16	3.9, 5.9, 8.2
	23	8.2

nominal heat flux by more than about 2%. Also, the subcooling never differed from the nominal 5°C by more than about 1.5°C. Therefore, the presentation of this data in this paper refers to the nominal values only.

3.7. Uncertainties

Table 2 shows the uncertainties for the calculated quantities used in this paper. Appendix A of Snyder [11] contains a listing of the first-order uncertainties of the equipment used and the degree to which the measurements could be obtained. It also contains a complete outline of the calculations for the uncertainties listed in Table 2.

4. Results and discussion

The transient heater surface mean temperature and the heat flux were measured for a total of 5 s during each test. Of these, 2 s of data was taken before the drop to capture the terrestrial gravity data, and 3 s of data was taken after the drop to capture the microgravity data. Because the experiment typically impacted the drag shield floor approx. 1.5 s after release, only the data from $t = 0$ to $t = 3.5$ s was plotted. As discussed later, 1.5 s of microgravity time was found to be adequate due to the application of an external forced field. The variation in the heat flux during the tests never exceeded $\pm 0.5\%$ from the set value and was assumed constant. Also, the heat flux was assumed to be equal to the instantaneous current through the heater multiplied by the instantaneous voltage [11].

4.1. Heater surface superheat

The heater surface superheat was calculated by subtracting the saturation temperature at the respective system pressure from the measured instantaneous surface mean temperature. Figs. 4–6 plot the heater surface superheats for the three electrode geometries with a nominal heat flux of 3.9 W/cm^2 and at voltages of 10 and 16 kV. Figs. 7–9 plot the heater surface superheats for the three electrode geometries with a nominal heat flux of 5.9 W/cm^2 and at voltages of 10 and 16 kV. Finally, Fig. 10 plots the heater surface superheats for all three electrode geometries with a nominal heat flux of 8.2 W/cm^2 and at voltages of 16 and 23 kV. The surface superheat without an electric field is also plotted on each figure at the respective nominal heat flux. This is the baseline curve which is provided for comparison and shows what the surface temperature would be without the pumping action provided by the dielectrophoretic forces.

The arrow on each graph represents the release and the start of microgravity. Therefore, the initial condition for each of the drops is terrestrial boiling at the respective heat flux. This initial condition was used because of the relatively long time it takes to nucleate (i.e. longer than the drop time). However, the magnitude of the DEP force was large enough that the initial conditions had little observable effect. As shown in Figs. 4–10, it is clear that the effect of the initial condition is no longer a factor after at most 0.5 s into microgravity due to the dominance of the electric field, which takes over when the gravity is absent. This initial condition allowed both terrestrial gravity and microgravity results together with the effects from the DEP forces to be viewed on one plot.

Note that for all the heat fluxes the surface temperature without the imposed DEP forces increased after the drop. The surface temperature increases more at the higher heat fluxes, i.e. 12, 16, and 32°C for heat fluxes of 3.9, 5.9, and 8.2 W/cm^2, respectively. As will be shown in the visualization section of this paper, the increase in surface temperature was due to the bubbles coalescing above the heater surface and forming large dry regions across the heater surface. The dryout area increased as the heat flux increased. In the tests at heat flux of 3.9 W/cm^2, shown in Figs. 4–6 the heater surface superheat with an electric field decreased in microgravity for the diverging-plate and flat-plate electrodes

Table 2
Experimental uncertainty

Item	Reference value	Uncertainty
Heat flux, Q''	4–8 W/cm^2	± 0.03 W/cm^2
Surface temperature, T_s	40°C	± 1.04°C
High voltage, V	12–23 kV	± 0.25 kV
Heat transfer coefficient, h	1200–2500 W/m^2 °C	± 150 W/m^2 °C

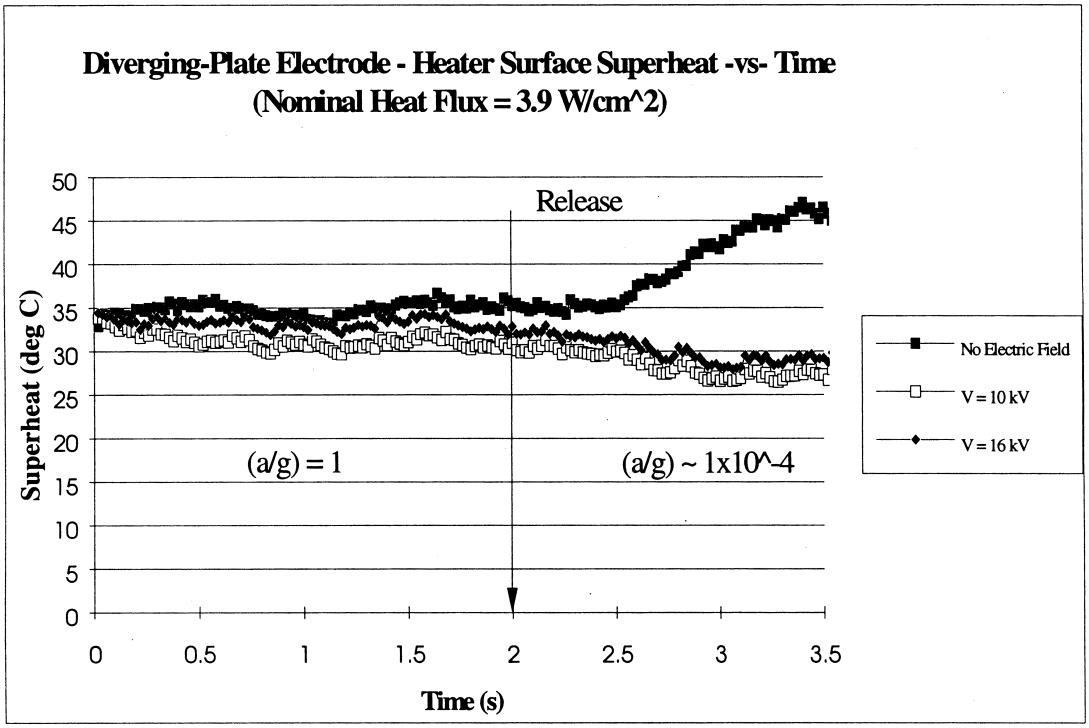

Fig. 4. Heater surface temperature superheat vs time for the diverging-plate electrode at a heat flux of 3.9 W/cm^2.

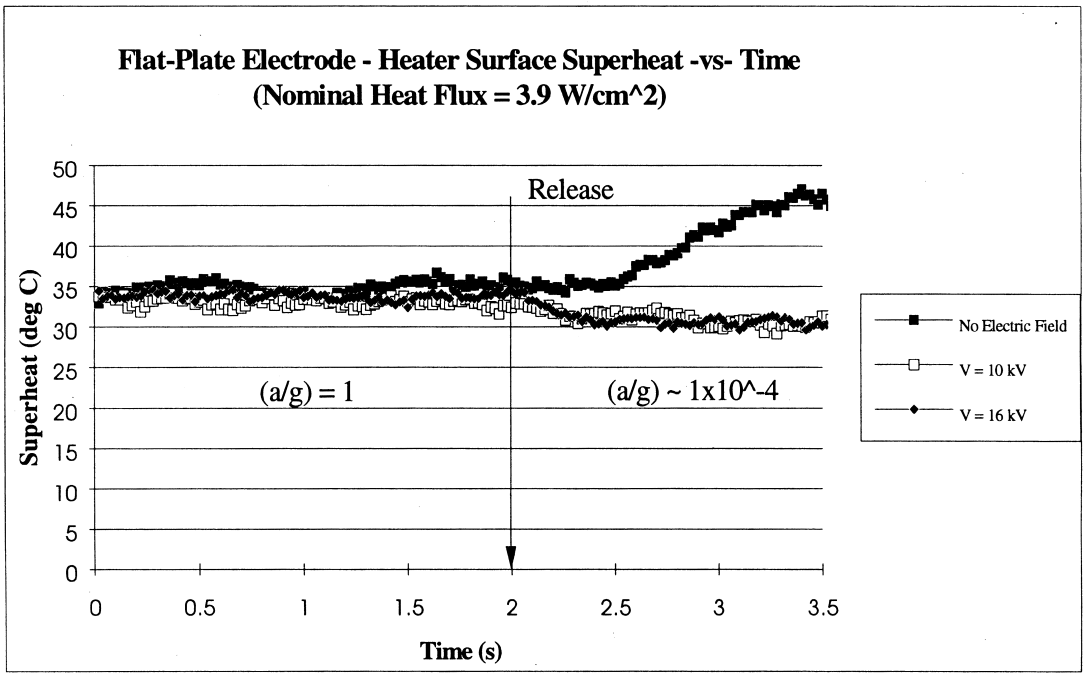

Fig. 5. Heater surface temperature vs time for the flat-plate electrode at a heat flux of 3.9 W/cm^2.

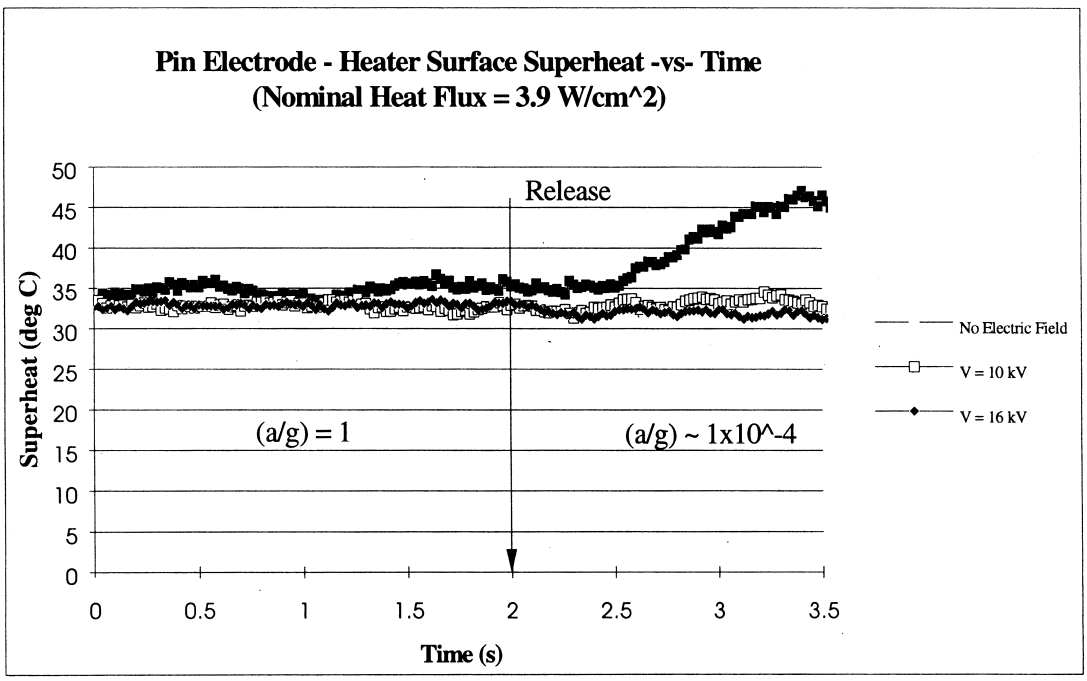

Fig. 6. Heater surface temperature vs time for the pin electrode at a heat flux of 3.9 W/cm^2.

and remained nearly constant for the pin electrode. In the test at a heat flux of 5.9 W/cm^2 as shown in Figs. 7–9 the heater surface superheat in microgravity remained nearly constant for the diverging-plate tests while for the flat-plate tests it increased slightly, and for the pin-electrode tests it increased even more

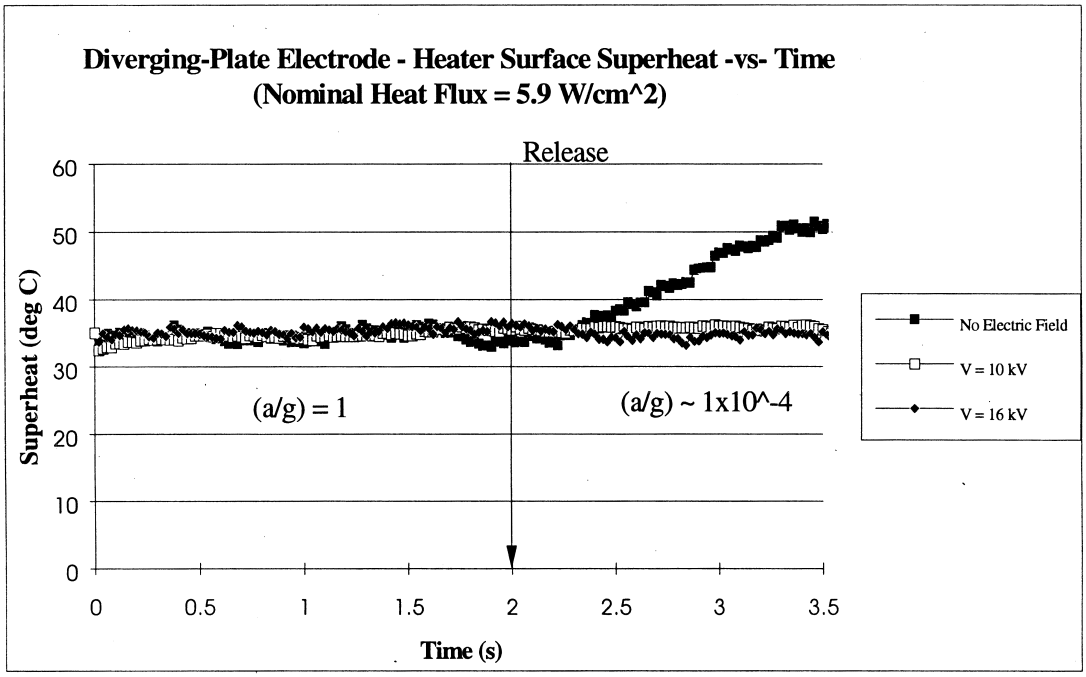

Fig. 7. Heater surface temperature vs time for the diverging-plate electrode at a heat flux of 5.9 W/cm^2.

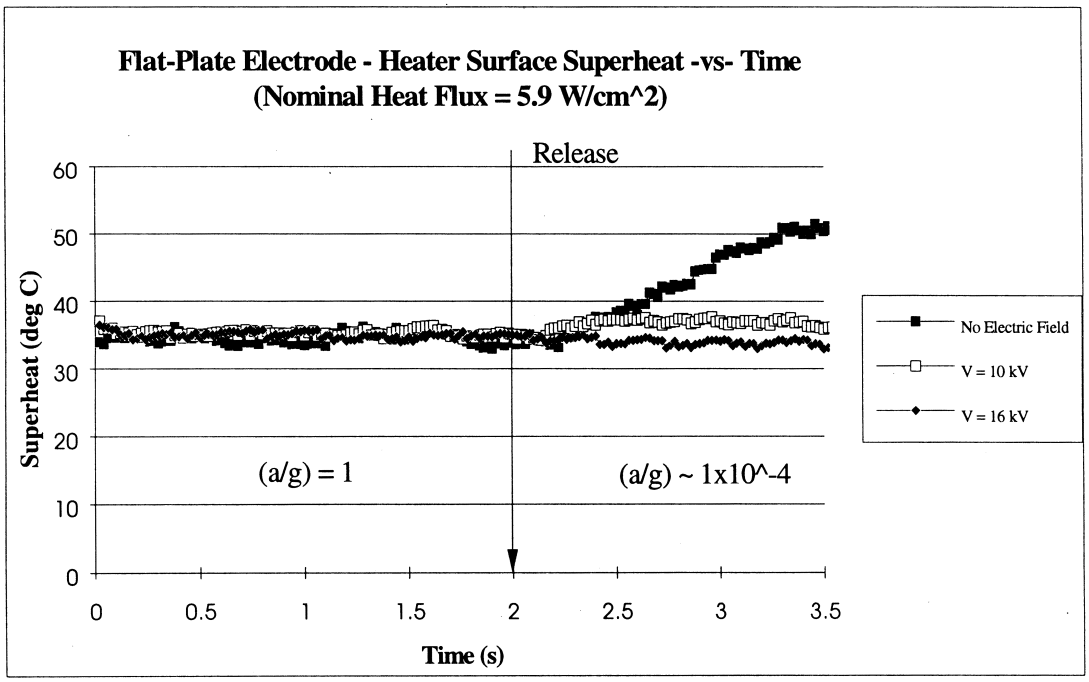

Fig. 8. Heater surface temperature vs time for the flat-plate electrode at a heat flux of 5.9 W/cm^2.

(about 5°). Finally, all three electrode geometries are plotted in Fig. 10 for the heat flux of 8.2 W/cm^2. For this highest heat flux, heater surface superheats in all the tests increased during microgravity, however, the largest increases were found with the pin electrode. Notice that the surface temperature can, in general, be

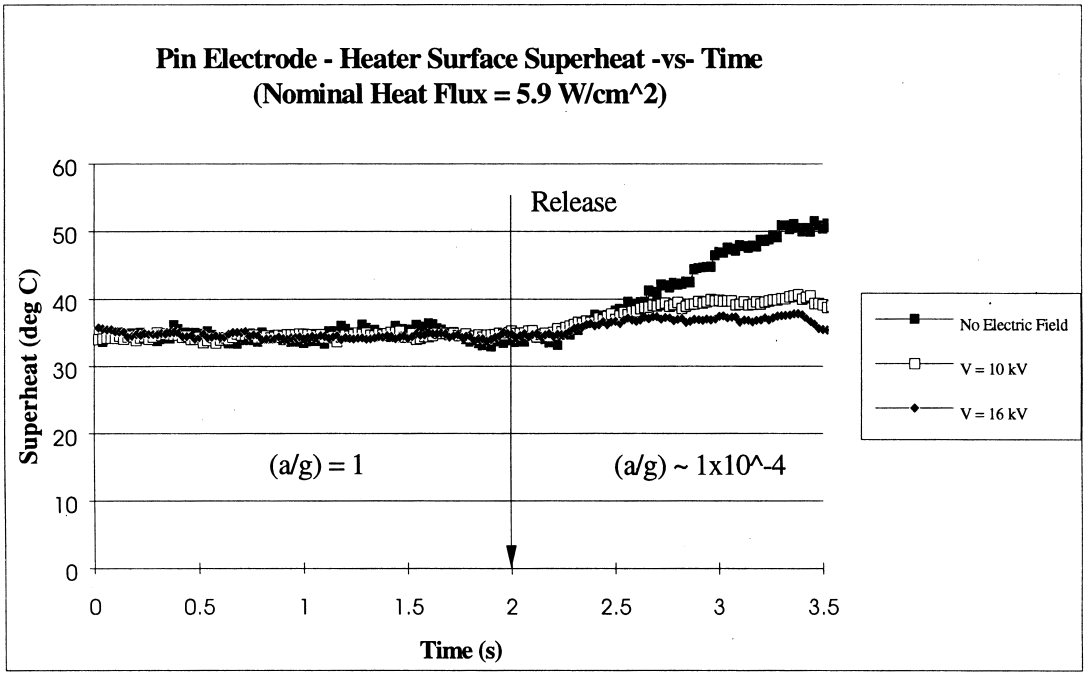

Fig. 9. Heater surface temperature vs time for the pin electrode at a heat flux of 5.9 W/cm^2.

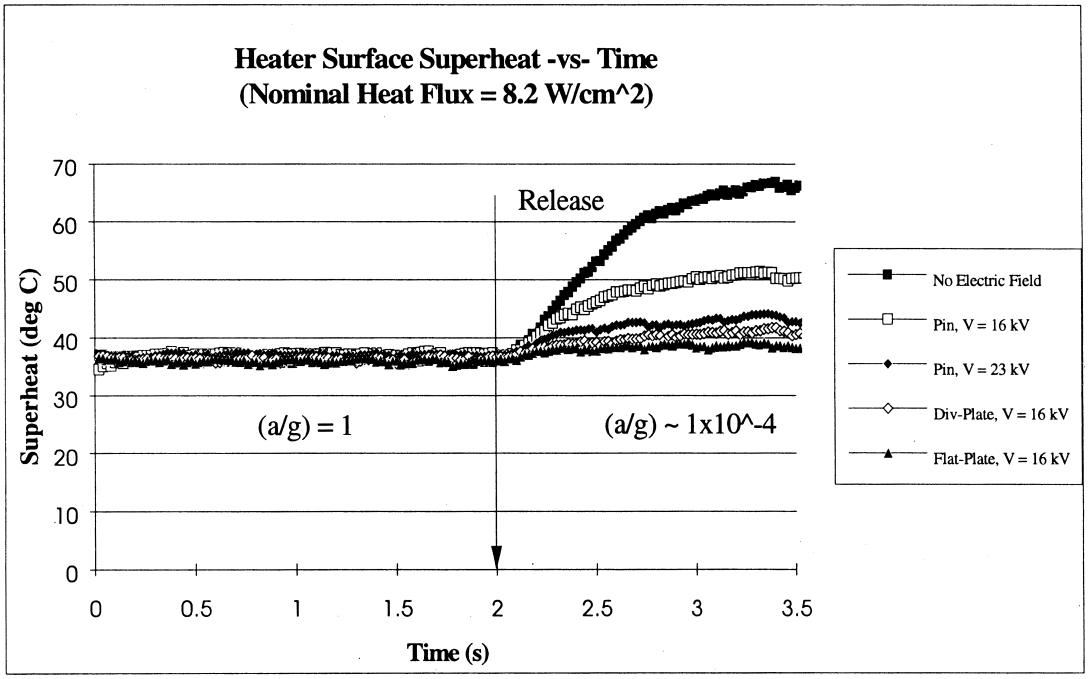

Fig. 10. Heater surface temperature vs time for all three electrodes at a heat flux of 8.2 W/cm^2.

reduced for any of the tests by simply increasing the high-voltage level. This is clearly shown in Figs. 6, 9, and 10 for the pin electrode.

4.2. Heat transfer coefficient

The average heat transfer coefficient, h, is defined as Q'' divided by the temperature difference between T_s and $T_{sat(nom)}$. Here, Q'' is the heat flux level, T_s is the instantaneous average heater surface temperature, and $T_{sat(nom)}$ is the nominal saturation temperature for the respective measured system pressure. Again, since the heat loss to the surroundings in nucleate boiling represents a very small portion of the total power input, the total heat flux was used to calculate the heat transfer coefficient.

Figs. 11 and 12 show the steady state heat transfer coeficients for different geometries under 10 and 16 kV, respectively. Again they demonstrate that the divergent plate is the most efficient, the flat plate is next, and the pin electrode is the least efficient. But consistently for both electric field strengths the flat plate geometry became more efficient than the divergent plate at higher heat fluxes. It is interesting to note that at lower heat fluxes, the heat transfer coefficient is not a strong function of the electric field strength, while at higher heat fluxes, the heat transfer coefficient increases with increasing electric field strength.

4.3. Visualization study

The visualization study was performed using two CCD cameras with a frame rate of 30 per second, and a shutter speed of 1/500 s. The heater surface and the electrodes were manufactured to be semi-transparent in order to facilitate the bottom view visualization. However, the lighting was not strong enough for the diverging plate tests, and was so drastically nonuniform for the flat-plate tests that good pictures could not be obtained over the entire heater surface. However, the lighting was adjusted for the pin electrode tests where the best bottom view was obtained. Finally, the back lighting allowed for visualization of the large bubbles which formed in microgravity, however, this did not produce sharp images during terrestrial gravity.

Figs. 13–16 show the side and bottom views of boiling process for terrestrial gravity and microgravity (1.5 s after release) without an electric field and at nominal heat fluxes of 3.9 and 8.2 W/cm^2. Figs. 17–19 show the side and bottom views of microgravity boiling at a heat flux of 3.9 W/cm^2 with a 10 or 16 kV electric field for the diverging-plate, flat-plate and pin electrodes. Fig. 20 shows the side and bottom views of microgravity boiling at a heat flux of 5.9 W/cm^2 with a 16 kV electric field for the pin electrode only. Fig. 21 shows the side and bottom views of microgravity boiling at a heat flux of 8.2 W/cm^2 with a 16 kV electric

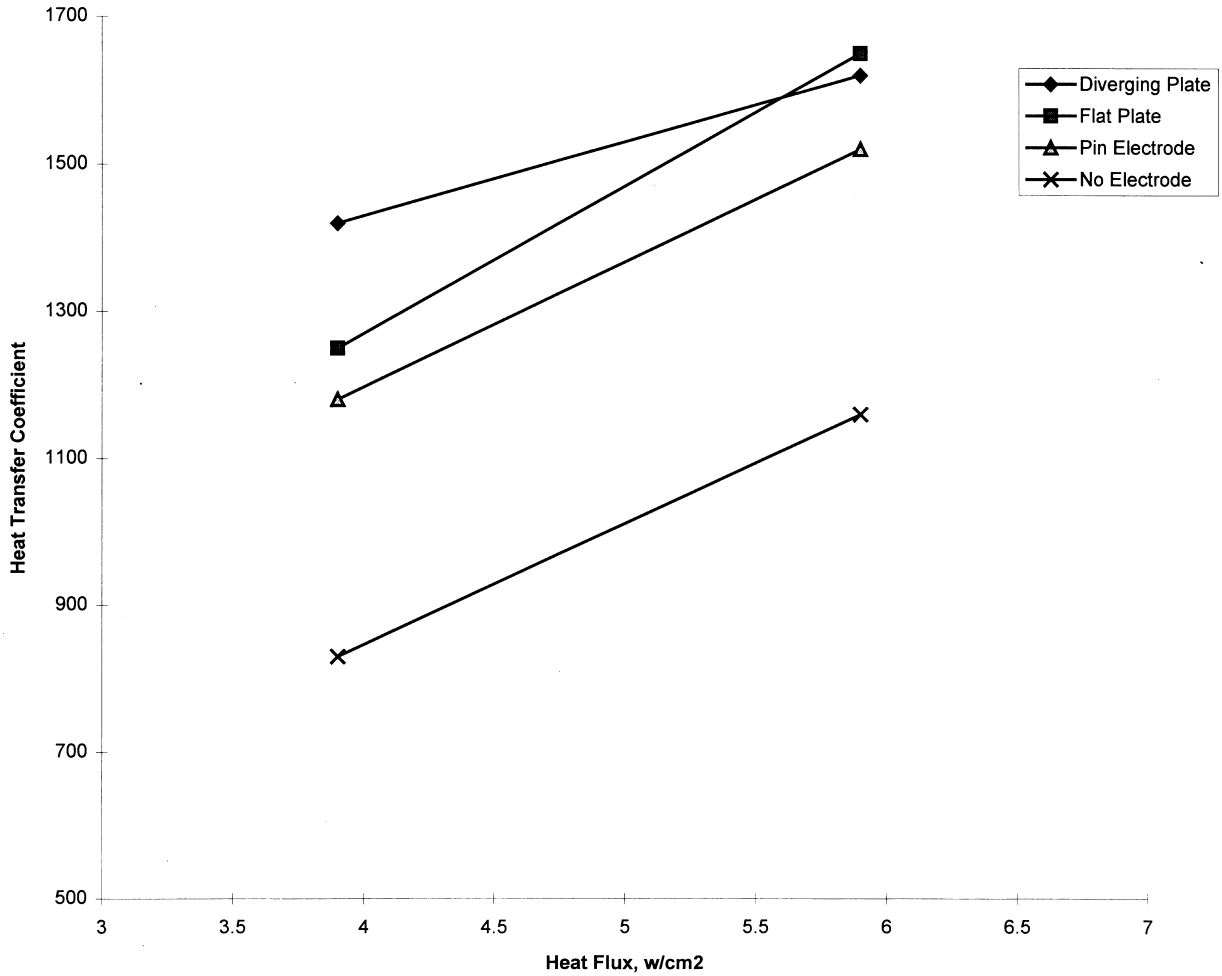

Fig. 11. Heat transfer coefficient vs heat flux for a 10 kV electric field.

field for the flat-plate electrode. Figs. 22 and 23 show the side and bottom views of microgravity boiling at a heat flux of 8.2 W/cm^2 for the pin electrode with 16 and 23 kV electric field, respectively.

From the previous heater surface superheat and heat transfer results, we might expect to see the highest degree of drying for the pin electrode — the pin electrode tests resulted in the highest average surface temperatures keeping other things constant. As can be seen in the figures this was the case. The pin electrode produced the largest DEP forces, however, the forces were very localized and decayed quickly moving away from the pin. The electric field is strongest directly under the pin and decays radially out from the pin. Therefore, as can be seen from the bottom view, the bubbles moved in a "flower" pattern, beginning small very near the pin electrode and growing and sliding radially away from the pin. Note that at the heat flux of 8.2 W/cm^2 under a 16 kV electric field a substantial amount of the heater surface near the edges is covered by vapor. However, for the same heat flux with 23 kV the vapor is kept from collecting and drying the heater.

The flat-plate electrode heat transfer coefficient typically fell somewhere between the pin electrodes and the diverging-plate electrodes. Near the edges of the plates, the gradient in the electric field is relatively strong and provided excellent pumping at this location, however, this force was localized similar to the pin electrode. Unlike the pin electrode, it did appear that the edge of the plate electrode was able to move all the bubbles away from the heater surface and no drying can be seen at these locations. However, directly under the flat-plate electrode the electric field is very uniform. This uniform electric field region results in an area where there is very little or no DEP force on the bubbles. The bottom view of this area was impossible to visualize, how-

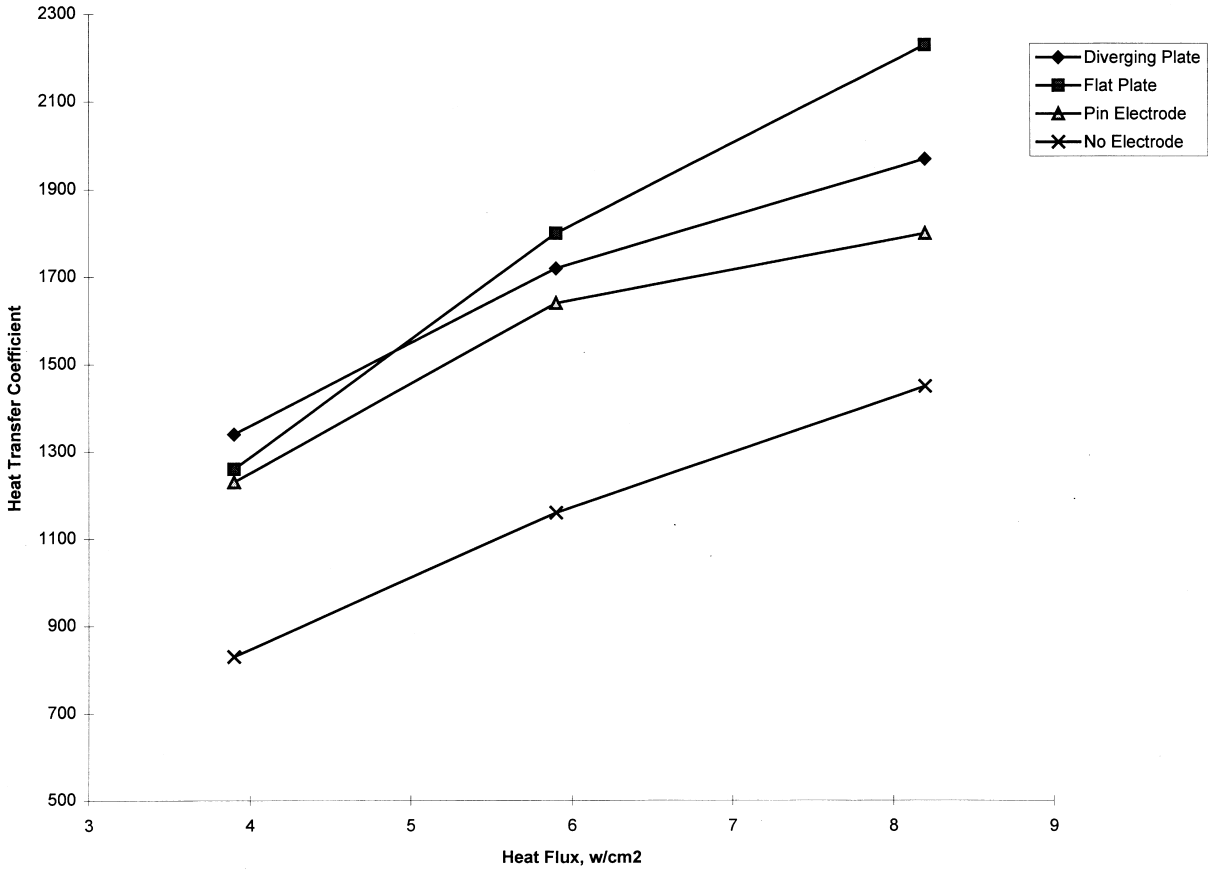

Fig. 12. Heat transfer coefficient vs heat flux for a 16 kV electric field.

ever, from the side view it does appear that this region has a substantial amount of stationary vapor above the heater surface. Also, based on the relatively high average surface temperatures measured, it is evident that some portion of the heater experienced some drying at the higher heat fluxes and lower voltages.

For the diverging-plate electrodes, the heat transfer coefficient was typically the highest relative to the other two electrode geometries under similar conditions, i.e. the average surface temperature was the lowest. The DEP force for this geometry pushed the bubbles across the heater surface similar to what one might experience with a forced flow.

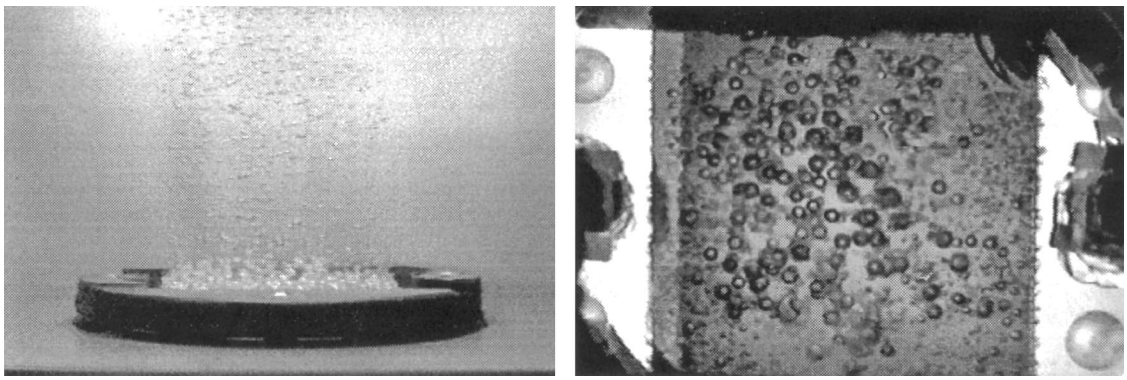

Fig. 13. Flow visualization of terrestrial gravity boiling with no electric field and a heat flux of 3.9 W/cm^2.

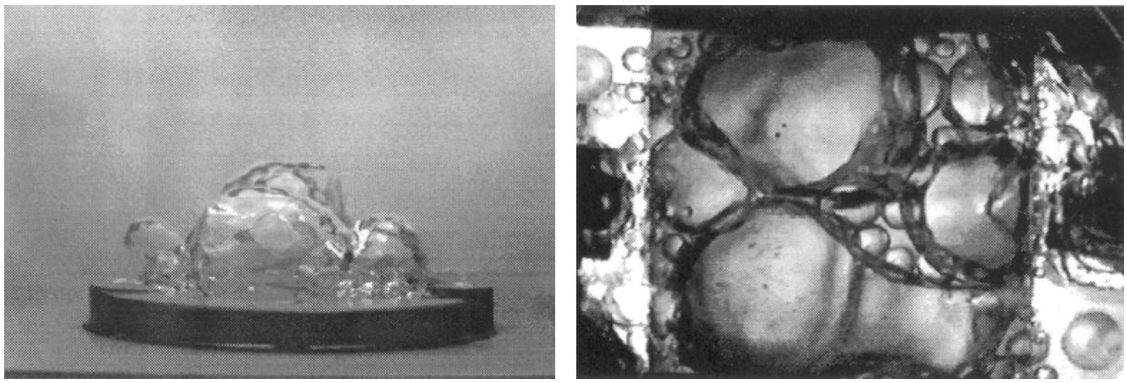

Fig. 14. Flow visualization of microgravity boiling with no electric field and a heat flux of 3.9 W/cm^2.

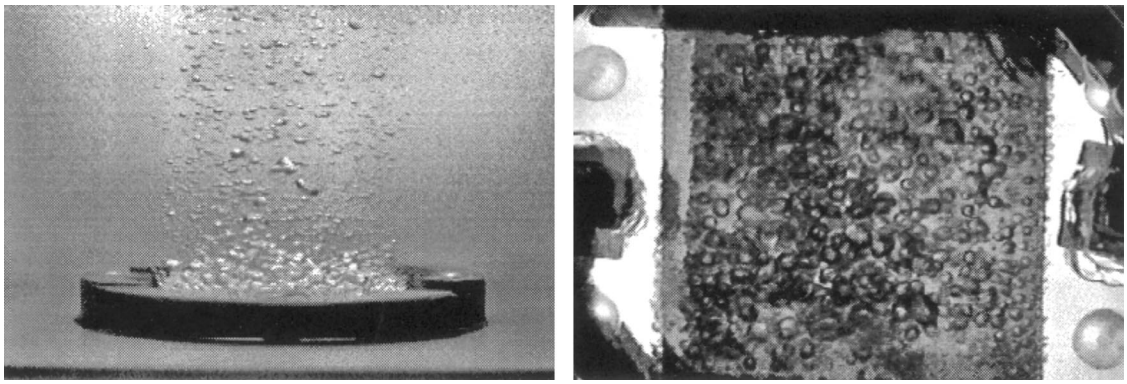

Fig. 15. Flow visualization of terrestrial gravity boiling with no electric field and a heat flux of 8.2 W/cm^2.

Ignoring edge effects, the DEP force was strongest at locations where the diverging plate was closest to the heater surface. The bubbles appeared to detach with relatively smaller diameters at this location (to the right in the pictures). After detaching, the bubbles moved across the heater surface and continued to slide and coalesce with other bubbles. In the region where the plates are the furthest apart (to the left in the pictures), one might think that the DEP force would be the weakest, however, the edge effects tend to dominate in this region and provide an additional DEP force [11]. Also, due to the edge effects on the left side (where the plates are closest together) the bubbles will again experience an

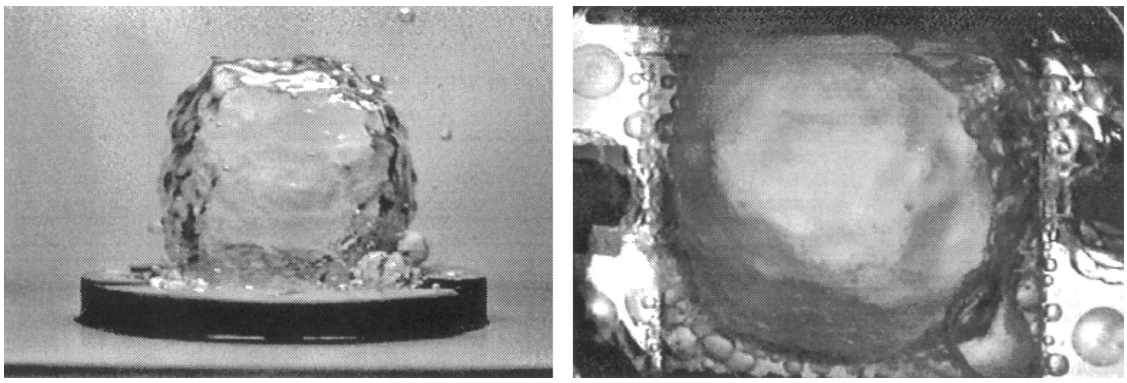

Fig. 16. Flow visualization of microgravity boiling with no electric field and a heat flux of 8.2 W/cm^2.

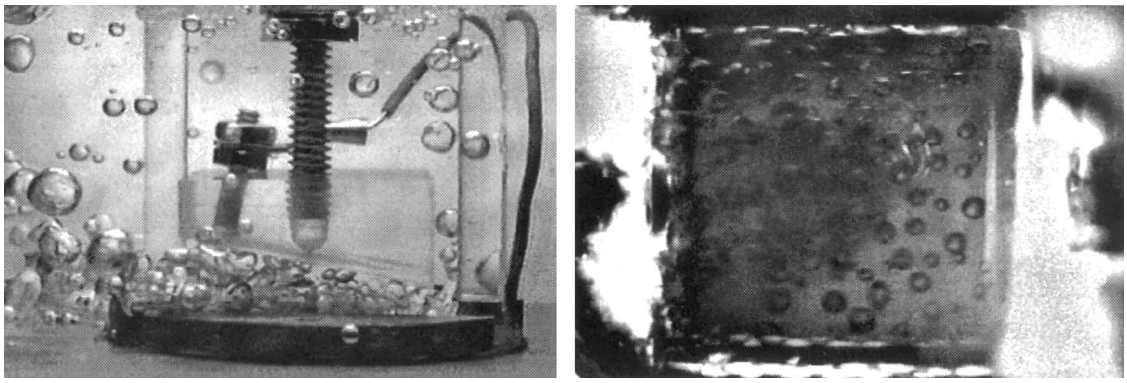

Fig. 17. Flow visualization of microgravity boiling for the diverging-plate electrode and a 16 kV electric field at a heat flux of 3.9 W/cm^2.

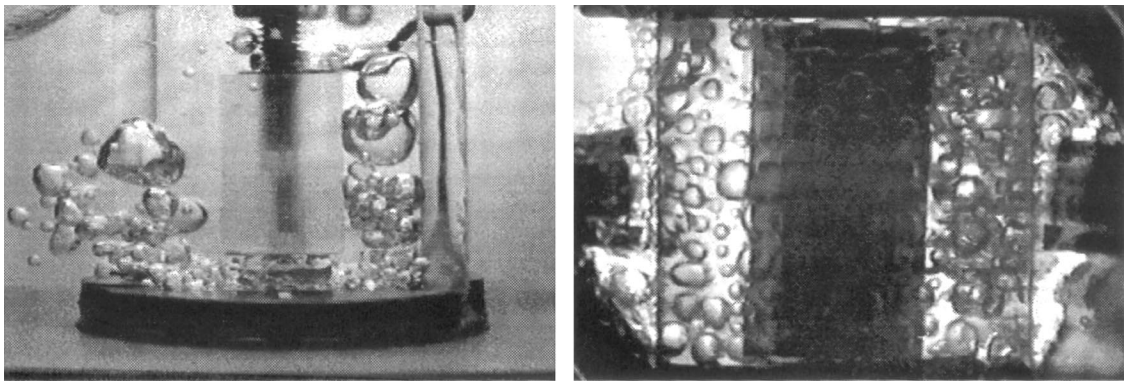

Fig. 18. Flow visualization of microgravity boiling for the flat-plate electrode and a 10 kV electric field at a heat flux of 3.9 W/cm^2.

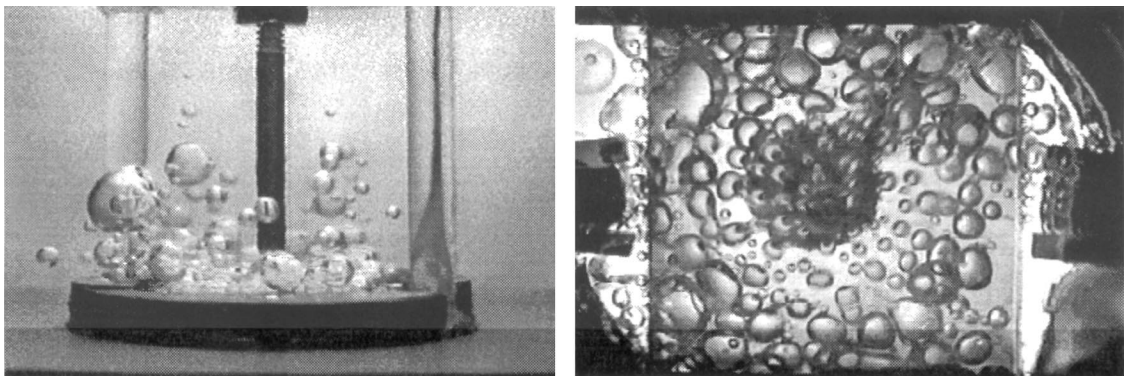

Fig. 19. Flow visualization of microgravity boiling for the pin electrode and a 16 kV electric field at a heat flux of 3.9 W/cm^2.

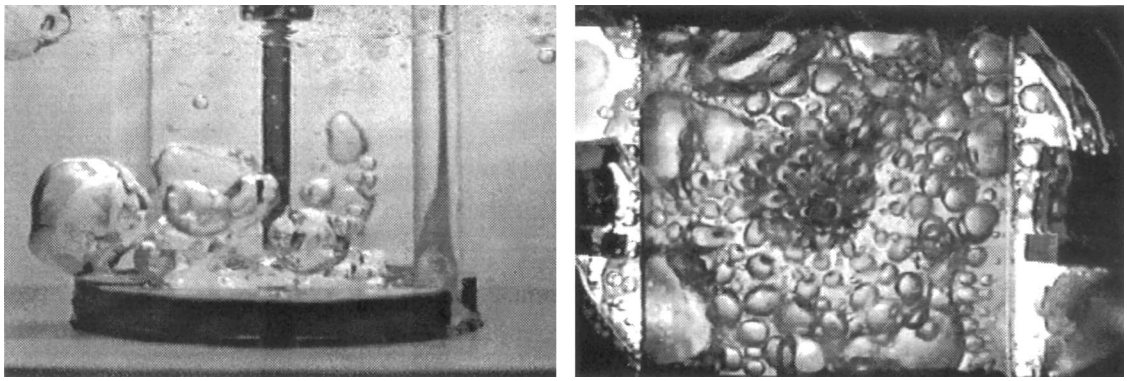

Fig. 20. Flow visualization of microgravity boiling for a pin electrode and a 16 kV electric field at a heat flux of 5.9 W/cm^2.

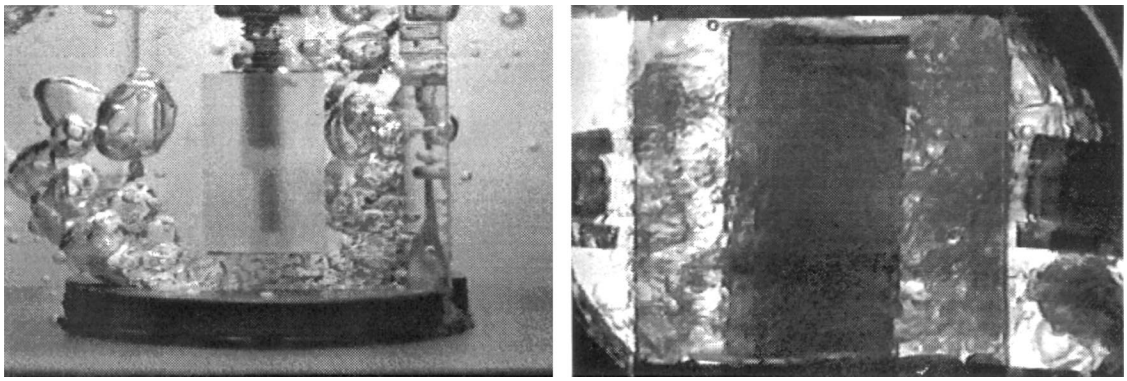

Fig. 21. Flow visualization of microgravity boiling for a flat-plate electrode and a 16 kV electric field at a heat flux of 8.2 W/cm^2.

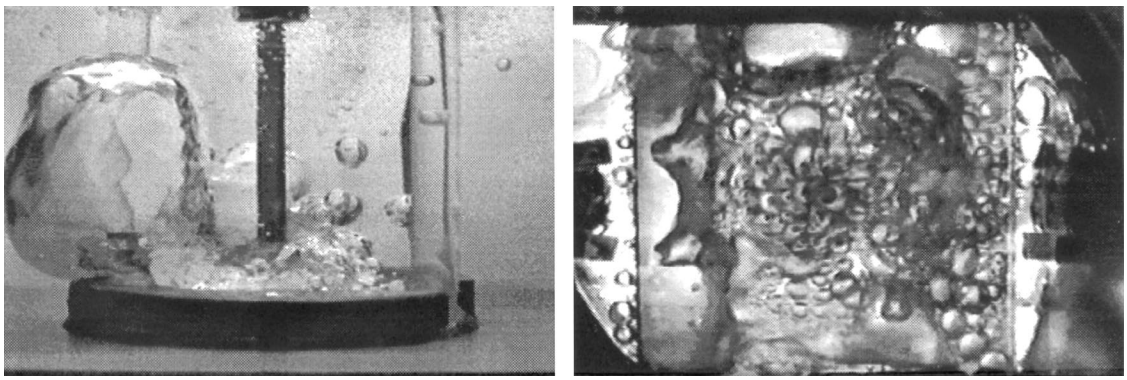

Fig. 22. Flow visualization of microgravity boiling for a pin electrode and a 16 kV electric field at a heat flux of 8.2 W/cm^2.

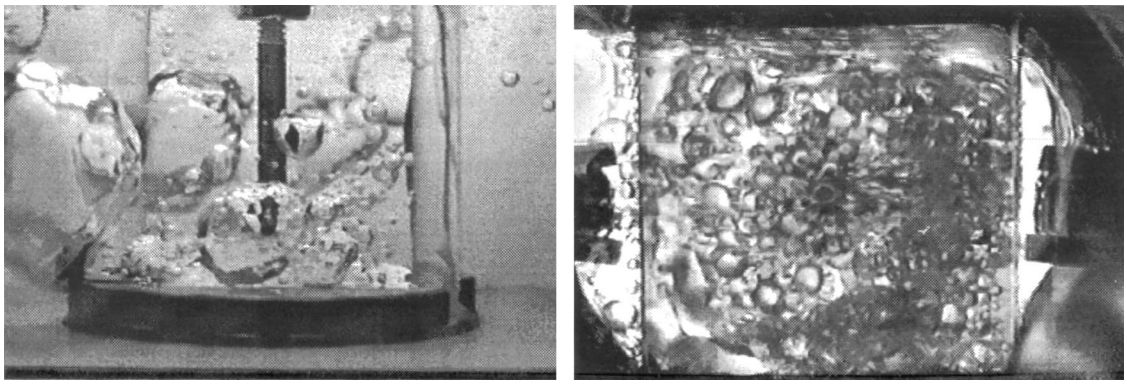

Fig. 23. Flow visualization of microgravity boiling for a pin electrode and a 23 kV electric field at a heat flux of 8.2 W/cm^2.

increased DEP force that will tend to push some of the bubbles out of the plates in the opposite direction. This phenomena was visualized in all the diverging-plate results.

Based on a digital image analysis, we estimated the mean bubble diameters and standard deviations for three typical cases. The results are:

Fig. 14, no electrode, mean bubble diameter = 73 mm, SD = 18 mm.

Fig. 17, divergent electrode, mean bubble diameter = 0.95 mm, SD = 0.2 mm.

Fig. 19, pin electrode, mean bubble diameter = 1.32 mm, SD = 0.6 mm.

We were unable to perform the image analysis for the flat plate geometry. It is again confirmed from the above image analysis that the average bubble size is smaller for the more efficient geometry.

5. Conclusion

In order to maintain steady nucleate boiling in microgravity another force must be imposed onto the boiling process to replace the gravity-driven buoyancy force. Using three electrode geometries it was found that an electric field can provide a replacement force for buoyancy in microgravity. Because the DEP force is dependent on the gradient of the electric field, any electrode geometry which produces large forces, inevitably results in the forces being more localized. Therefore specific geometries must be developed and used in order to maximize the effectiveness of an electric field in microgravity.

The effectiveness of an electrode geometry could be quantified by a parameter which is simply the ratio of the heat transfer coefficient in microgravity to the heat transfer coefficient in terrestrial gravity. If this parameter is unity the effectiveness of an electric field is the same as that of the terrestrial gravity. If this parameter is less than unity or greater than unity the effectiveness of an electric field is less than the terrestrial gravity or more than the terrestrial gravity, respectively. For the cases investigated, the effectiveness is the highest for the diverging-plate electrode geometry and lowest for the pin geometry for all the heat flux levels and voltages. It is greater than unity for all three electrode geometries at the heat flux level of 3.9 W/cm^2. For the heat flux level of 5.9 W/cm^2, it is roughly unity for the diverging-plate and flat-plate geometries and slightly less than unity for the pin geometry. For the highest heat flux of 8.2 W/cm^2, the value of effectiveness is always less than unity for all three geometries. In general, the effectiveness is higher for 16 kV than for 10 kV. Therefore, an electric field can be as effective or more effective than the terrestrial gravity if the voltage is high enough.

Acknowledgements

The research was supported by NASA Grant NAG3-1387. Dr Fran Chiaramonte was the project monitor, who provided constant support. The first author was a NASA Graduate Student Researcher Program Fellow for 3 years.

References

[1] J. Straub, M. Zell, B. Vogel, Pool boiling in a reduced gravity field, Proceedings of the International Heat Transfer Conference 1 (1990) 91–112.

[2] J.S. Ervin, H. Merte, R.B. Keller, K. Kirk, Transient pool boiling in microgravity, Int. J. Heat Mass Transfer 35 (1992) 659–674.

[3] H.S. Lee, H. Merte, F. Chiaramonte, 1996. The pool boiling curve in microgravity, AIAA paper 96-0499.

[4] J.A. Stratton, Electromagnetic Theory, McGraw-Hill, New York, 1941 (chap. 2).
[5] H.A. Pohl, Dielectrophoresis, the Behavior of Neutral Matter in Nonuniform Electricfields, Cambridge University Press, Cambridge, 1987.
[6] T.B. Jones, G.W. Bliss, Bubble dielectrophoresis, Journal of Applied Physics 48 (4) (1976) 1412–1417.
[7] T.B. Jones, Electrodynamically enhanced heat transfer in liquids — a review, in: T.F. Irvine, J.P. Hartnett (Eds.), Advances in Heat Transfer, vol. 14, Academic Press, New York, 1978.
[8] P.D.I. Marco, W. Grassi, Saturated pool boiling enhancement by means of an electric field, J. of Enhanced Heat Transfer 1 (1) (1993) 99–114.
[9] K.J. Cheng, J.B. Chaddock, Effect of an electric field on bubble growth rate, Int. Comm. Heat Mass Transfer 12 (1985) 259–268.
[10] D.M. Pachosa, J.N. Chung, Dielectrophoresis-driven nucleate boiling in a simulated microgravity environment, ASME J. Heat Transfer 115 (1993) 495–498.
[11] T.J. Snyder. Studies on the dielectrophoretic force and its effects on boiling bubble dynamics and heat transfer in terrestrial and microgravity environments, Ph.D. dissertation, Washington State University, 1995.
[12] T.J. Snyder. WSU 2.1 — second microgravity drop tower: design, construction, and performance, M.S. thesis, Washington State University, 1993.
[13] Fluorinert, Electronic Liquids, Product Manual, 3M Co., 1990.
[14] E. Oker, H. Merte Jr, Semi-transparent gold film as simultaneous surface heater and resistance thermometer for nucleate boiling studies, J. of Heat Transfer 103 (1981) 65–68.